CRYSTAL GROWTH & DESIGN

ARTICLE

pubs.acs.org/crystal

Zone Leveling Crystal Growth of Thermoelectric PbTe Alloys with Sb_2Te_3 Widmanstätten Precipitates

Teruyuki Ikeda,[*,†,‡] Nathan J. Marolf,[‡] and G. Jeffrey Snyder[‡]

[†]PRESTO, Japan Science and Technology Agency, 4-1-8 Honcho, Kawaguchi, Saitama 332-0012, Japan

[‡]Materials Science, California Institute of Technology, 1200 California Boulevard, Pasadena, California 91125, United States

ABSTRACT: Unidirectional solidification of PbTe-rich alloys in the pseudobinary PbTe-Sb_2Te_3 system using the zone leveling technique enables the production of large regions of homogeneous solid solutions for the formation of precipitate nanocomposites as compared with Bridgman solidification. $(PbTe)_{0.940}(Sb_2Te_3)_{0.060}$ and $(PbTe)_{0.952}(Sb_2Te_3)_{0.048}$ alloys were successfully grown using $(PbTe)_{0.4}(Sb_2Te_3)_{0.6}$ and $(PbTe)_{0.461}(Sb_2Te_3)_{0.539}$ as seed alloys, respectively, with 1 mm h^{-1} withdrawal velocity. In the unidirectionally solidified regions of both alloys, Widmanstätten precipitates are formed due to the decrease in solubility of Sb_2Te_3 in PbTe. To determine the compositions of the seed alloys for the zone leveling experiments, the solute distribution in solidification in the PbTe-richer part of the pseudobinary PbTe-Sb_2Te_3 system has been examined from the concentration profiles in the samples unidirectionally solidified by the Bridgman method.

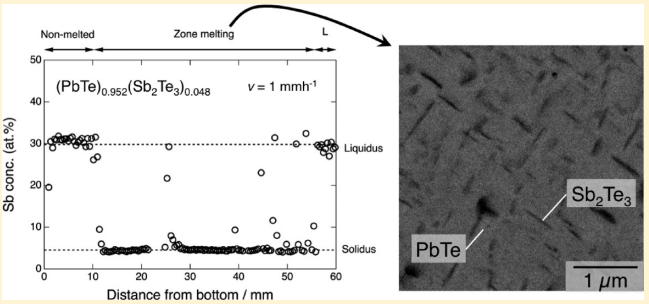

1. INTRODUCTION

The efficiency of thermoelectric conversion depends on the dimensionless figure of merit zT, defined as $S^2\sigma T/\kappa$, where S is the Seebeck coefficient, σ is the electrical conductivity, and κ is the thermal conductivity, expressed as $\kappa = \kappa_{ele} + \kappa_{lat}$, where κ_{ele} and κ_{lat} stand for thermal conduction by electrons and lattice, respectively. The increase of zT leads to improved efficiency in thermoelectric conversion. Since zT depends on materials, we can expect an increasing emphasis on the development of advanced thermoelectric materials.

Nanostructuring is one of the important routes to reduction of κ_{lat} leading to enhanced zT of bulk thermoelectric materials.[1−3] For some nanostructured PbTe-based materials, which are regarded as promising materials for applications in temperature ranges up to 500 °C,[4] including PbTe-$AgSbTe_2$[5] and PbTe-Ag_2Te,[6] their very low lattice thermal conductivities are connected to nanoprecipitates. Controlling the nanostructure of these materials based on their phase diagrams and phase transformations has been regarded as an essential field of research.

Many thermoelectric materials are fabricated by processes based on powder metallurgy because of their poor mechanical properties. Because of the relatively high grain boundary density, there could be significant influence on the microstructure formation. For example, precipitation may preferentially occur on grain boundaries and hence result in a nanostructure that differs from that in materials with large grain size. On the other hand, usual solidification processing, which normally results in larger grain structures, is often associated with the formation of cast defects such as shrinkage cavities. Unidirectional solidification can fabricate alloys with large grain size (or single crystals depending on conditions and materials) and less crystal defects allowing us to precisely control the microstructure on the basis of transformation theories.

Zone leveling technique is known as a method which enables us to unidirectionally grow crystals at a constant composition.[7] For fabrication of thermoelectric materials, there are several studies found in the literature; examples include studies on Bi_2Te_3,[8] Si−Ge,[9,10] and Zn_4Sb_3.[11]

For the pseudobinary PbTe-Sb_2Te_3 system, we have reported that unidirectional solidification by the Bridgman method results in the formation of the PbTe base alloy with Sb_2Te_3 Widmanstätten precipitates.[12] However, because of the solute distribution in solidification, the ratio of the yield to the total amount of charge (size of sample produced) is limited to a few millimeters. While large PbTe samples with precipitates can be obtained by normal solidification processing followed by homogenization and post heat treatments,[13] better quality alloys with less cast defects are desired. In this work, we demonstrate unidirectional solidification using a zone leveling technique to obtain large homogeneous PbTe base alloys with constant compositions in the pseudobinary PbTe-Sb_2Te_3 system (the latest phase diagram is presented in ref 14). In order to properly conduct zone leveling experiments, the solute distribution in solidification needs to be studied. While the liquidus line for the PbTe-rich region in the PbTe-Sb_2Te_3 system has been studied,[15−17] the solidus line has not been examined. Therefore, we experimentally determine the

Received: June 15, 2011
Revised: July 26, 2011
Published: August 03, 2011

solute distribution in solidification in the PbTe-rich part of the phase diagram of the PbTe-Sb_2Te_3 system as well.

2. EXPERIMENTAL SECTION

2.1. Determination of Solute Distribution in Solidification. Four alloys with the initial compositions listed in Table 1 were synthesized by melting Pb, Sb, and Te (99.999% purity) at 1223 K for 600 s in fused quartz tubes with a 6 mm inner diameter under Ar at 3.4×10^4 Pa. The compositions of these alloys are on the pseudobinary PbTe-Sb_2Te_3 line and in the range where the primary solidification is supposed to be with the PbTe phase.[15] Unidirectional solidification experiments by the Bridgman method were performed with 0.3 mm h^{-1} velocity. The alloys were lowered downward in a temperature gradient of ~27 K mm^{-1} (at temperatures close to the melting temperatures). The samples were cut lengthwise in half with a diamond saw and the inner cross sections were polished with a series of SiC papers up to #800 and then polished with a series of Al_2O_3 powder (3−0.3 μm). The chemical composition was measured as a function of the distance from the bottom end of the sample using a wavelength dispersive X-ray spectrometer (WDS, JXA-8200, JEOL Ltd.) with Sb and PbTe samples as standards for ZAF correction[18] from intensities of Pb M_α, Sb L_α, and Te L_α to concentrations. The accelerating voltage was 15 kV. To determine the average composition of heterophase microstructure, which is formed by the solid-state precipitation, the probe diameter was set to 25 μm.

2.2. Zone Melting Experiments. Ampules used for the zone melting experiments were prepared by the following procedure. The composition of seed alloy for each sample alloy was chosen based on the solute distribution data obtained in the former part of this work so that the primary solidification of the seed alloys occurs at the targeted compositions. By starting the zone melting experiment from the seed alloy in each experiment, the alloy with the targeted composition can be grown continuously if the unidirectional solidification proceeds with single phase (zone leveling effect[7]). The sample and seed alloys with the compositions listed in Table 2 were synthesized by melting Pb, Sb, and Te at 1223 K for 600 s in fused quartz tubes with a 12 mm inner diameter under Ar at 3.4×10^4 Pa. The compositions of these alloys (both samples and seeds) are on the pseudobinary PbTe-Sb_2Te_3 line. The alloys were then smashed into small pieces.

The seed alloy was sealed under Ar at 3.4×10^4 Pa in a fused quartz with 6 mm inner and 10 mm outer diameters, melted, and solidified by air-cooling. The small pieces of the sample alloy, with the targeted composition in Table 2, were then loaded into the same ampule and sealed under Ar. (The targeted composition is here defined as the composition at which the solid phase is supposed to be grown in each experiment if the unidirectional solidification proceeds with single phase. It is typically the same as the sample composition in zone leveling experiments.) The end of the ampule containing the sample alloy with the targeted composition was placed into a furnace up to the point of the seed alloy at the opposite end. The sample alloy was melted and then solidified by being poured onto the top of the seed alloy by flipping the ampule upside down, followed by immediate water-quenching. The approximate weight and length are 7.5 g and 35 mm for the seed alloy (bottom) and 14.5 g and 65 mm for the sample alloy (top).

The set up for the zone melting experiments is shown in Figure 1. A part of the alloy is melted by induction heating with a spiral coil (13 mm inner diameter). Upper and lower parts of the melt zone are cooled by air flow to control the length of the melt zone and enhance the steepness of the temperature gradients. The heated and cooled zones are separated by fused quartz plates with 13 mm spacing. An ampule is loaded in the system so that the boundary between the seed and sample alloy is located at the position of the top fused quartz plate. The heating power is chosen so that the liquid/solid interfaces are located around the fused quartz plates. Then, the ampule is lowered downward with a constant velocity (1 or 10 mm h^{-1}). During the experiment, the ampule is turned at a

Table 1. Compositions of Alloys Used in Unidirectional Solidification by the Bridgman Method[a]

sample ID	initial composition (atom %)	solidus composition (atom %)
BM-1	$Pb_{17.8}Sb_{29.8}Te_{57.4}$	$Pb_{44.4}Sb_{4.5}Te_{51.1}$
	$(PbTe)_{46.2}(Sb_2Te_3)_{53.8}$	$(PbTe)_{95.2}(Sb_2Te_3)_{4.8}$
BM-2	$Pb_{15.2}Sb_{27.8}Te_{57.0}$	$Pb_{44.6}Sb_{4.3}Te_{51.1}$
	$(PbTe)_{52.2}(Sb_2Te_3)_{47.8}$	$(PbTe)_{95.4}(Sb_2Te_3)_{4.6}$
BM-3	$Pb_{17.6}Sb_{25.9}Te_{56.5}$	$Pb_{46.3}Sb_{3.0}Te_{50.7}$
	$(PbTe)_{57.6}(Sb_2Te_3)_{42.4}$	$(PbTe)_{96.9}(Sb_2Te_3)_{3.1}$
BM-4	$Pb_{20}Sb_{24}Te_{56}$	$Pb_{46.8}Sb_{2.5}Te_{50.6}$
	$(PbTe)_{62.5}(Sb_2Te_3)_{37.5}$	$(PbTe)_{97.4}(Sb_2Te_3)_{2.6}$

[a] The right column lists the composition of primary solidification, which is regarded as solidus composition for each alloy. The compositions in pseudo-binary notation are shown in the second lines.

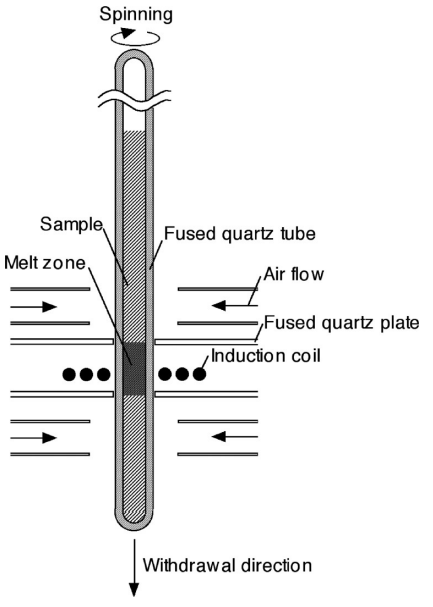

Figure 1. Set up for the zone melting experiments.

Table 2. Conditions of the Zone Melting Experiments[a]

sample ID	sample composition (targeted composition) (atom %)	seed composition (atom %)	velocity/mm h^{-1}
ZM5.5Sb-1	$Pb_{43.1}Sb_{5.5}Te_{51.4}$ $(PbTe)_{0.940}(Sb_2Te_3)_{0.060}$	none	10
ZM5.5Sb-2	$Pb_{43.1}Sb_{5.5}Te_{51.4}$ $(PbTe)_{0.940}(Sb_2Te_3)_{0.060}$	$Pb_{10.5}Sb_{31.6}Te_{57.9}$ $(PbTe)_{0.4}(Sb_2Te_3)_{0.6}$	10
ZM5.5Sb-3	$Pb_{43.1}Sb_{5.5}Te_{51.4}$ $(PbTe)_{0.940}(Sb_2Te_3)_{0.060}$	$Pb_{10.5}Sb_{31.6}Te_{57.9}$ $(PbTe)_{0.4}(Sb_2Te_3)_{0.6}$	1
ZM4.5Sb	$Pb_{44.4}Sb_{4.5}Te_{51.1}$ $(PbTe)_{0.952}(Sb_2Te_3)_{0.048}$	$Pb_{12.8}Sb_{29.8}Te_{57.4}$ $(PbTe)_{0.461}(Sb_2Te_3)_{0.539}$	1

[a] The compositions in pseudo-binary notation are shown in the right columns.

dx.doi.org/10.1021/cg2007588 |Cryst. Growth Des. 2011, 11, 4183–4189

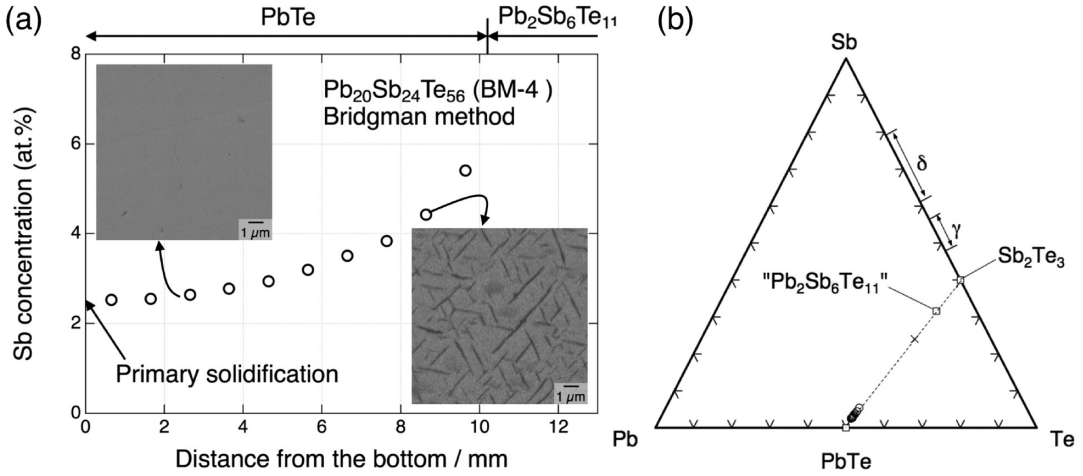

Figure 2. Concentration variation in $Pb_{20}Sb_{24}Te_{56}$ alloy, which was unidirectionally solidified by the Bridgman method with 0.3 mm h^{-1} velocity. The micrographs shown in the profile versus the distance from the bottom of the sample (a) show the microstructures at the corresponding positions. Panel (b) shows the ternary plot for the composition variation.

constant rate. The temperature distribution is measured with an optical pyrometer (Modline 5, IRcon Corp.).

After zone melting, the samples were cut lengthwise in half and the inner cross sections were prepared for microstructure observations in the same manner as mentioned above. The final polishing was done with colloidal silica (0.05 μm). The microstructure was observed using a field emission-scanning electron microscope (FE-SEM, Carl Zeiss LEO 1550 VP) equipped with a backscattered electron detector. The accelerating voltage was 20 kV. The chemical composition was measured as a function of the distance from the bottom end of the sample by WDS. To determine the average composition of heterophase microstructure, the probe diameter was set to 25 μm.

3. RESULTS AND DISCUSSION

3.1. Solute Distribution in Solidification. For all of the alloys used in the unidirectional solidification experiments to determine the distribution coefficient by the Bridgman method (BM-1 to 4), PbTe was crystallized at the bottom as the primary solidification phase, consistent with previous studies.[12,15] Figure 2 shows an example of the concentration profiles of the primary solidification regions (sample: BM-4). In this sample, the Widmanstätten structure (with PbTe matrix and Sb_2Te_3 plate precipitates), which has been reported previously,[12] is observed in the high Sb concentration region ($c_{Sb} \gtrsim 3$ atom %), while just a few precipitates are found in the region with lower Sb concentrations. The average composition measured with 25 μm probe size, which is larger than the microstructure size, shifts monotonically to the Sb_2Te_3-richer direction, until "$Pb_2Sb_6Te_{11}$" is crystallized by the peritectic reaction. (The chemical formula "$Pb_2Sb_6Te_{11}$" was first used by Abrikosov et al.[15] However, the crystal structure has been reported to be $PbSb_2Te_4$.[19] Therefore, quotation marks are used for this chemical formula in this paper.) The bottom end of the alloy is crystallized when the majority of the alloy is still in the liquid state with the composition very close to the initial composition. Therefore, if the chemical diffusion in cooling after solidification does not affect the compositional variation reflecting the solute distribution much, the composition at the bottom end is regarded as the solidus composition against the liquidus

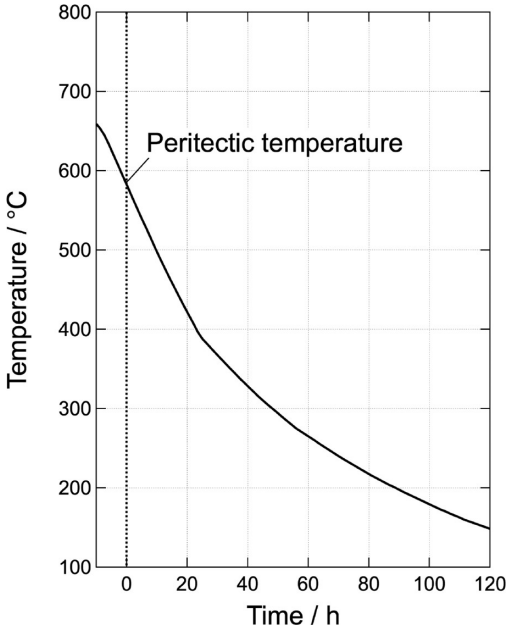

Figure 3. Temperature variation with time evaluated from the temperature distribution in the furnace and the velocity of sample withdrawal in the unidirectional solidification by the Bridgman method.

composition which equals the initial composition of the alloy. Figure 3 shows the temperature variation with time at a constant position in a sample during the unidirectional solidification, evaluated from the temperature distribution and the velocity of the sample. On the basis of the cooling curve, the diffusion distance x is roughly estimated to be ~10 μm using $x = (\int_0^{t_\infty} D(t)\, dt)^{1/2}$, where $D(t)$ is the diffusivity of atoms which depends on temperature and hence time t. In the estimation, the diffusion coefficient of Sb in PbTe[20] was used. Thus, the diffusion distance is much smaller than the length scale of the compositional variation due to the solute distribution in solidification (Figure 2), allowing us to determine the primary solidification composition as that at the bottom. Figure 4 plots the Sb concentration of the solidus against the initial Sb concentration in the alloy. The numerical

dx.doi.org/10.1021/cg2007588 |Cryst. Growth Des. 2011, 11, 4183–4189

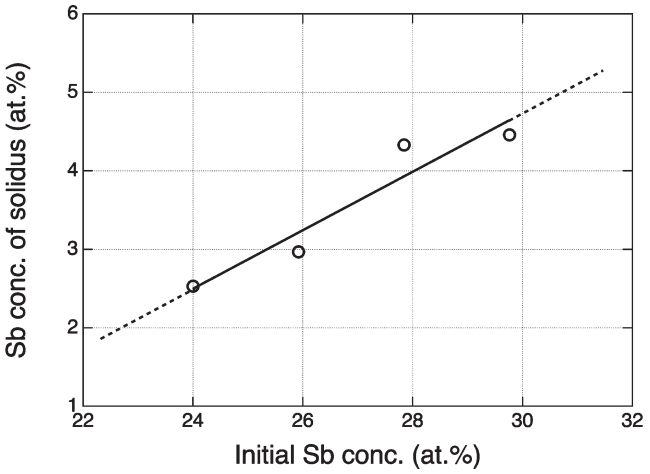

Figure 4. The relation between the initial sample composition (BM-1 to BM-4) and the composition where the primary solidification occurs (solidus composition). The line drawn in the graph is a guide for the eyes.

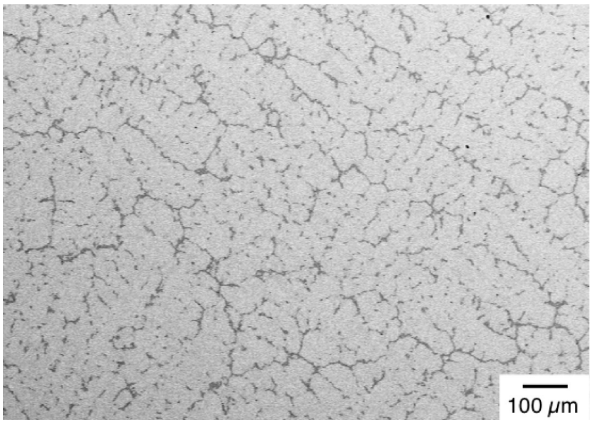

Figure 5. Microstructure of $Pb_{43.1}Sb_{5.5}Te_{51.4}$ alloy before the zone melting experiment of ZM5.5Sb-1.

data are given in Table 1. The Sb concentration increases by increasing the initial Sb concentration as expected.

3.2. Zone Leveling Effect. Before zone melting experiments, the samples are solidified by pouring onto the top of the seed materials and immediate water-quenching of the entire ampules. After this process, the microstructure is dendritic as shown in Figure 5. The size scale of the dendrite structure is tens of micrometers in the order of magnitude.

Figure 6 shows the microstructure of zone-melted alloys. In each row in the figure, the image on the right-hand side shows the microstructure taken with higher magnification than those on the left-hand side. The compositional variation in the alloys, measured with a 25 μm probe, is plotted as a function of the distance from the bottom end in Figure 7.

Without a seed material (ZM5.5Sb-1, Figure 7a), the solute was diluted by the zone refining effect. The velocity of the sample withdrawal is 10 mm h^{-1}. The solute concentration (<3 atom % Sb) is lower than the targeted composition (broken line). Because of the low solute concentration, there is no solid-state precipitation observed (Figure 6a). With the same velocity (v = 10 mm h^{-1}) and

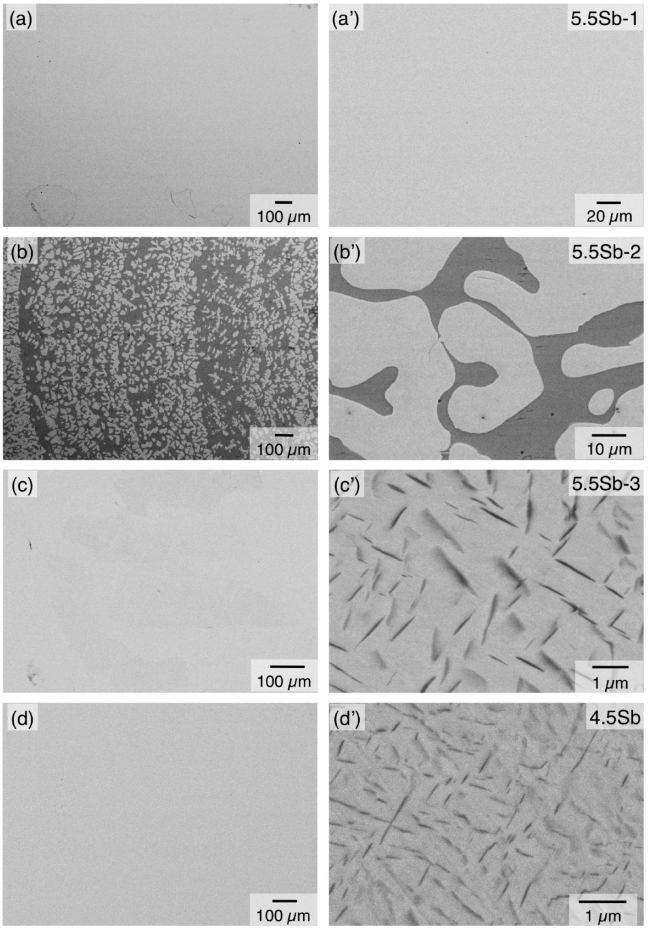

Figure 6. Microstructures of the zone-melted regions in ZM5.5Sb-1 (a, a'), ZM5.5Sb-2 (b, b'), ZM5.5Sb-3 (c, c'), and ZM4.5Sb (d, d'). The images on the right-hand side show those with higher magnification.

with the seed material (ZM5.5Sb-2, Figure 7b), the solute concentration was higher than the targeted composition. This is related to the observation that the solidification microstructure is dendritic as shown in Figure 6b. This means that in the solidification the solid/liquid interface was not flat. If the formation of dendrites is due to constitutional supercooling, it can be avoided for the conditions in which the relation is held:[21]

$$\frac{G}{vc_0} > m\frac{1-k_0}{Dk_0} \quad (1)$$

where G, v, c_0, m, k_0, and D are the temperature gradient, solidification velocity, targeted composition, tangential slope of liquidus, distribution coefficient, and diffusion coefficient of solute, respectively. For a given composition in a given material system, what can readily be manipulated is G or v. In the next experiment, v is reduced to 1 mm h^{-1}.

With the decreased velocity 1 mm h^{-1} and the same seed sample as ZM5.5Sb-2, the concentration of the solute is held close to the targeted level in large portions of the zone melted region (ZM5.5Sb-3, Figure 7c) suggesting that the velocity of 1 mm h^{-1} is slow enough to allow the solute elements to diffuse well in the melt zone. This makes the gradient of the solute concentration so small that the condition expressed by eq 1 is satisfied. From this experimental fact, the diffusion coefficient of solute in liquid can roughly be estimated to be 10^{-8}–10^{-7} m^2/s

dx.doi.org/10.1021/cg2007588 |*Cryst. Growth Des.* 2011, 11, 4183–4189

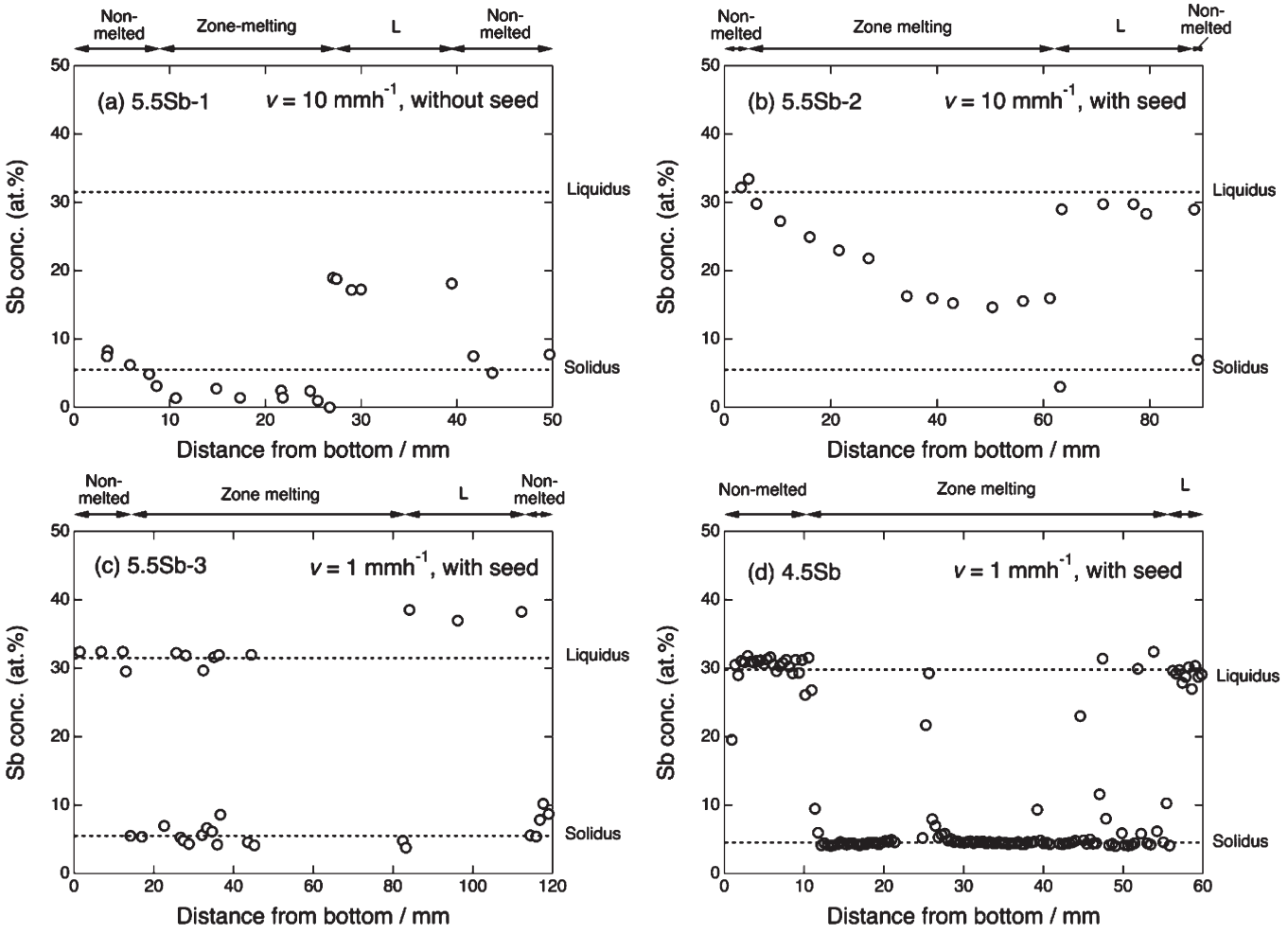

Figure 7. Concentration profiles after zone melting experiments of ZM5.5Sb-1 (a), ZM5.5Sb-2 (b), ZM5.5Sb-3 (c), and ZM4.5Sb (d). The zone melted region is indicated at the top of each graph.

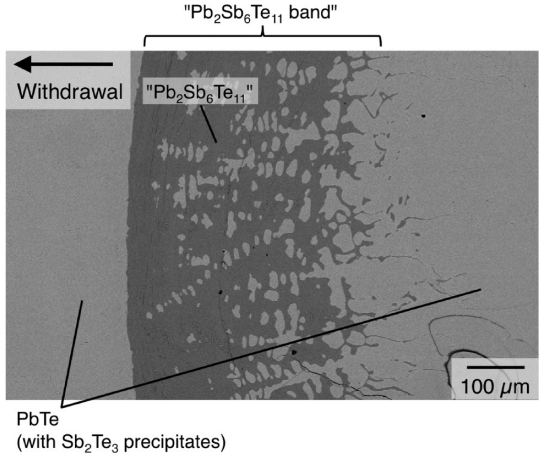

Figure 8. A "$Pb_2Sb_6Te_{11}$ band" with PbTe dendrites observed in ZM5.5Sb-3.

since the range of D is derived from eq 1 as $v_1c_0m(1 - k_0)/k_0/G < D < v_2c_0m(1 - k_0)/k_0/G$, where v_1 and v_2 are 1 and 10 mm h^{-1}. In the estimation, the following parameters were used: $c_0 = 5.5$ atom % Sb, $k_0 = 0.17$, $G = 1-10$ K mm^{-1}, and $m \sim 10$. Here, k_0 was calculated as the ratio of the solidus to the liquidus (5.5 to 31.5 atom % Sb), and m was roughly estimated from the previous phase diagram.[15] The diffusion coefficients in liquid metals typically fall into the range within an order from 5×10^{-9} m^2 s^{-1}.[22] The diffusivity we obtain here agrees with this empirical law.

As Figure 7c shows, the alloy is partly solidified with the composition of the seed material. The microstructure of such regions is shown in Figure 8. The region with the seed material ($Pb_{10.5}Sb_{31.6}Te_{57.9}$) forms a "band" perpendicularly to the withdrawal direction, in which the solidification microstructure is similar to that previously observed in a solidification study with higher cooling rates (air- or water-cooling).[23] Therefore, such regions were presumably solidified with higher cooling rates than other regions. Because the composition of liquidus in equilibrium with the targeted composition (~5.5 atom % Sb) is close to the peritectic composition (~32 atom % Sb[15]), supercooling due to a higher cooling rate could result in the solidification with the peritectic phase "$Pb_2Sb_6Te_{11}$". The fluctuation of the cooling rates is attributed to the temperature instability, which could be related to the variation in the heating efficiency, reflecting the existence of such crystal defects as cracks in the solid part of the samples.

To avoid the formation of the peritectic phase, the temperature of the melt zone should be controlled in a more stable fashion (i.e., using a susceptor) or the melt composition in equilibrium with the targeted composition has to be farther from the

dx.doi.org/10.1021/cg2007588 |Cryst. Growth Des. 2011, 11, 4183–4189

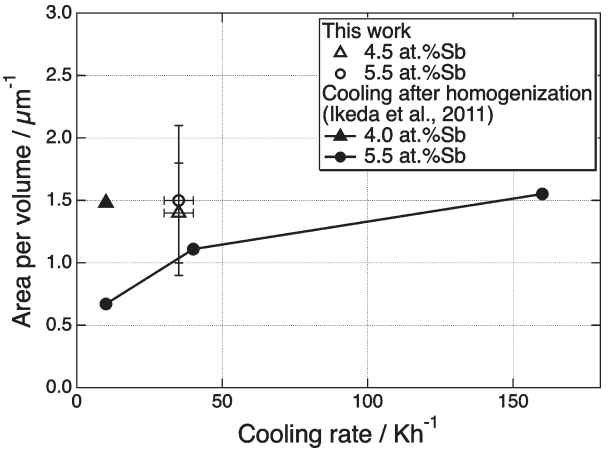

Figure 9. Area per unit volume of the plate precipitates of ZM4.5Sb (4.5 atom % Sb) and ZM5.5Sb-3 (5.5 atom % Sb) compared with that of alloys cooled with constant rates after homogenization.[13] Error range corresponds to statistic errors from analyses of multiple images.

peritectic composition so that the solidification temperature at the targeted composition will be increased. The sample composition of ZM4.5Sb (~4.5 atom % Sb) is in equilibrium with the liquid with the composition ~29.8 atom % Sb, which is farther from the peritectic composition (~32 atom % Sb) than that the liquid which ZM5.5Sb (~5.5 atom % Sb) is in equilibrium with (~31.6 atom % Sb), as seen in Figure 4. A zone leveling experiment for ZM4.5Sb was performed using the seed material with the ~29.8 atom % Sb composition. As Figures 6d and 7d show, the alloy with the ~29.8 atom % Sb composition works well as the seed alloy for ZM4.5Sb. At this composition, an almost homogeneous alloy with the targeted composition was obtained except for only a few bands of the peritectic phase.

3.3. Formation of Widmanstätten Precipitates. The regions with the targeted compositions are uniformly formed of Widmanstätten precipitates of Sb_2Te_3 both in ZM5.5Sb-3 and ZM4.5Sb as shown in Figure 6, panels c′ and d′, respectively. The formation of the precipitates in the solid state is due to the decrease in the solubility of Sb_2Te_3 in PbTe.[12] The temperature gradient measured in the solid phase where the solidification interface has passed is 30−40 K mm^{-1}. From this temperature gradient and the velocity of 1 mm h^{-1}, the cooling rate is estimated to be 30−40 K h^{-1}. The micrographs taken by scanning electron microscopy were digitally analyzed in the way proposed in the previous work[13] to obtain the area per unit volume of the plate precipitates as shown in Figure 9. The results in this work agree in terms of the size scales of precipitates with those presented for the samples which were cooled in electrical furnaces after homogenization annealing[13] within error ranges. The relatively large error ranges could be attributed to the temperature instability. In previous work, it was concluded that the size scale of Widmanstätten precipitates can be regulated by controlling the rate of cooling or by modifying composition. The same method could be used to control the size of precipitates in a zone leveling method; the cooling rates can be regulated through the control of the withdrawal velocity of the material or temperature gradient. It should be noted, however, that there is a limit in velocity if the formation of dendrites needs to be avoided as discussed above.

It has been recognized that the formation of nanoprecipitates is effective for the reduction of the lattice thermal conductivity of thermoelectric materials. Since solid-state precipitation behavior is affected by the existence of grain boundaries, it is preferable to prepare samples with large grains by solidification processing in order to control the size scale of precipitates precisely. The advantage of the samples fabricated by the zone leveling technique is that they do not contain shrinkage cavities as much as those prepared by the normal solidification method since they are grown unidirectionally so that the degradation of mechanical and thermoelectric properties by the formation of cavities could be avoided.

4. CONCLUSIONS

Zone leveling is an ideal method to produce large homogeneous regions of supersaturated solid solutions for the formation of nanoscale precipitation composites. The solute distribution in solidification in the PbTe-richer part of the pseudobinary PbTe-Sb_2Te_3 system has been determined from the concentration profiles in the samples unidirectionally solidified by the Bridgman method. On the basis of the solute distribution, seed alloys of zone leveling experiments have been chosen: $Pb_{10.5}Sb_{31.6}Te_{57.9}$ seed to grow $Pb_{43.1}Sb_{5.5}Te_{51.4}$ and $Pb_{12.8}Sb_{29.8}Te_{57.4}$ seed to grow $Pb_{44.4}Sb_{4.5}Te_{51.1}$. Zone melting with the sample and seed alloy combinations and with 1 mm h^{-1} withdrawal velocity results in the formation of homogeneous primary solidification with PbTe crystal with the targeted concentrations of the solute. Sb_2Te_3 Widmanstätten precipitates form in PbTe during cooling in zone melting experiments due to the decrease in the solubility of Sb_2Te_3 in PbTe with temperature.

AUTHOR INFORMATION

Corresponding Author

*Tel.: +1-626-395-4814. Fax: +1-626-395-8868. E-mail: tikeda@caltech.edu.

ACKNOWLEDGMENT

This work was funded by the PRESTO program (PRESTO: Precursory Research for Embryonic Science and Technology) of Japan Science and Technology Agency. Microscopy facilities are supported by NSF CSEM MRSEC at Caltech.

REFERENCES

(1) Snyder, G. J.; Toberer, E. S. *Nat. Mater.* **2008**, *7*, 105–114.
(2) Medlin, D. L.; Snyder, G. J. *Curr. Opin. Colloid Interface Sci.* **2009**, *14*, 226–235.
(3) Kanatzidis, M. G. *Chem. Mater.* **2010**, *22*, 648–659.
(4) Wood, C. *Rep. Prog. Phys.* **1988**, *51*, 459–539.
(5) Hsu, K. F.; Loo, S.; Guo, F.; Chen, W.; Dyck, J. S.; Uher, C.; Hogan, T.; Polychroniadis, E. K.; Kanatzidis, M. G. *Science* **2004**, *303*, 818–821.
(6) Pei, Y.; Lensch-Falk, J.; Toberer, E. S.; Medlin, D. L.; Snyder, G. J. *Adv. Funct. Mater.* **2011**, *21*, 241–249.
(7) Pfann, W. G. *Zone Melting*; John Wiley and Sons, Inc: New York, 1958.
(8) Ha, H. P.; Hyun, D. B.; Byun, J. Y.; Oh, Y. J.; Yoon, E. P. *J. Mater. Sci.* **2002**, *37*, 4691–4696.
(9) Dismukes, J. P.; Ekstrom, L.; Steigmeier, E. F.; Kudman, I.; Beers, D. S. *J. Appl. Phys.* **1964**, *35*, 2899.
(10) Vining, C. B.; Laskow, W.; Hanson, J. O.; Van der Beck, R. R.; Gorsuch, P. D. *J. Appl. Phys.* **1991**, *69*, 4333–4340.
(11) Pedersen, B. L.; Iversen, B. B. *Appl. Phys. Lett.* **2008**, *92*, 161907.

(12) Ikeda, T.; Ravi, V. A.; Snyder, G. J. *Acta Mater.* **2009**, *57* 666–672.
(13) Ikeda, T.; Marolf, N. J.; Bergum, K.; Toussaint, M. B.; Heinz, N. A.; Ravi, V. A.; Snyder, G. J. *Acta Mater.* **2011**, *59*, 2679–2692.
(14) Ikeda, T.; Snyder, G. J. *Mater. Res. Soc. Symp. Proc.* **2010**, *1267*, DD06–07.
(15) Abrikosov, N. K.; Elagina, E. I.; Popova, M. A. *Inorg. Mater.* **1965**, *1*, 1944–1946.
(16) Hirai, T.; Takeda, Y.; Kurata, K. *J. Less-Common Met.* **1967**, *13* 352–356.
(17) Reynolds, R. A. *J. Electrochem. Soc.* **1967**, *114*, 526–529.
(18) Flewitt, P. E. J.; Wild, R. K. *Physical Methods for Materials Characterization*; Institute of Physics Publishing: Bristol and Philadelphia, 1994.
(19) Shelimova, L. E.; Karpinskii, O. G.; Svechnikova, T. E.; Avilov, E. S.; Kretova, M. A.; Zemskov, V. S. *Inorg. Mater.* **2004**, *40*, 1264–1270.
(20) Boltaks, B. I.; Makhov, Y. N. *Sov. Phys.-Techn. Phys.* **1958**, *3* 974–977.
(21) Rutter, J. W.; Chalmers, B. *Can. J. Phys.* **1953**, *31*, 15–39.
(22) Chalmers, B. *Principle of Solidification*; Wiley: New York, 1964.
(23) Ikeda, T.; Haile, S. M.; Ravi, V. A.; Azizgolshani, H.; Gascoin, F.; Snyder, G. J. *Acta Mater.* **2007**, *55*, 1227–1239.